Inorganic Chemistry

Article

pubs.acs.org/IC

Observation of the Inverse Trans Influence (ITI) in a Uranium(V) Imide Coordination Complex: An Experimental Study and Theoretical Evaluation

Oanh P. Lam,[†] Sebastian M. Franke,[†] Hidetaka Nakai,[‡] Frank W. Heinemann,[†] Wolfgang Hieringer,*[,§] and Karsten Meyer*[,†]

[†]Department of Chemistry and Pharmacy, Inorganic Chemistry, University of Erlangen-Nuremberg, Egerlandstraße 1, D-91058 Erlangen, Germany

[‡]Department of Chemistry and Biochemistry, Graduate School of Engineering, Kyushu University, 744 Moto-oka, Nishi-ku, Fukuoka 819-0395, Japan

[§]Department of Chemistry and Pharmacy, Theoretical Chemistry, University of Erlangen-Nuremberg, Egerlandstraße 3, D-91058 Erlangen, Germany

Supporting Information

ABSTRACT: An inverse trans influence has been observed in a high-valent U(V) imide complex, $[((^{Ad}ArO)_3N)U(NMes)]$. A thorough theoretical evaluation has been employed in order to corroborate the ITI in this unusual complex. Computations on the target complex, $[((^{Ad}ArO)_3N)U(NMes)]$, and the model complexes $[((^{Me}ArO)_3N)U(NMes)]$ and $[(NMe_3)(OMe_2)(OMe)_3U(NPh)]$ are discussed along with synthetic details and supporting spectroscopic data. Additionally, the syntheses and full characterization data of the related U(V) trimethylsilylimide complex $[((^{Ad}ArO)_3N)U(NTMS)]$ and U(IV) azide complex $[((^{Ad}ArO)_3N)U(N_3)]$ are also presented for comparison.

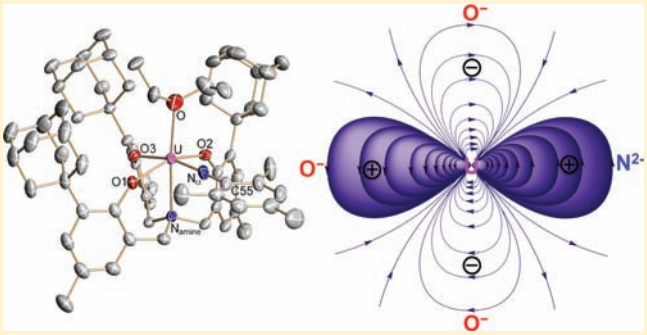

INTRODUCTION

Organic azides have been employed for the synthesis of mid- to high-valent metal azido (M−N_3) and imido (M═NR) complexes.[1] Both species are well-documented precursors to transition-metal nitrido complexes (M≡N);[2] however, despite many efforts, the synthesis and isolation of complexes with a terminal uranium nitrido unit, U≡N, has remained elusive in discrete molecular complexes.[3] The increased interest in uranium nitrido complexes stems from its potential to offer information on f orbital contribution in bonding, therefore providing insights into the properties of $(UN)_x$ materials for the development of new-generation nuclear fuels.[4] Attempts at isolating a discrete U≡N species have resulted in the formation of U−N clusters,[3b−d] capped nitrido species,[5] and the μ-nitrido dinuclear complexes $[\{([t\text{-Bu}]ArN)_3)U\}_2(\mu\text{-}N)]^{+/0/-}$.[6] More recently, Kiplinger et al. reported a fleeting and highly reactive U−N intermediate that underwent C−H activation with its supporting ligand.[7] It appears that a key challenge in promoting the formation of and stabilizing a mononuclear U−N unit lies in identifying a ligand with the appropriate steric and electronic environment.

Our continuous interest in high-valent metal complexes with terminal imido and nitrido units has now led to the isolation of an U(V) imide complex, $[((^{Ad}ArO)_3N)U(NMes)]$. Supported by the tris-aryloxide ligand $(^{Ad}ArO)_3N^{3-}$ (trianion of tris(2-hydroxy-3-adamantyl-5-methylbenzyl)amine), the U(V) imide complex $[((^{Ad}ArO)_3N)U(NMes)]$ exhibits an inverse trans influence, as evidenced by X-ray crystallography. The structural trans influence is well-documented in transition-metal complexes and is commonly found in square-planar and octahedral complexes.[8] It describes the phenomenon in which the M−L bond trans to a strongly bound ligand is effectively weakened, characterized by an elongation of that bond. The opposite occurs in complexes that exhibit an inverse trans influence (ITI), where the M−L bond trans to a strong anionic ligand is shortened.[9] As suggested by Denning, the inverse trans influence may be explained by the electrostatic interaction between the strong anionic ligand and the metal core electrons, resulting in a polarization of these electrons.[9] Following Denning's analysis, the polarization is dipolar when the highest filled core orbitals have opposite parity with respect to the valence shell orbitals.[9] When the core shell and valence shell orbitals possess the same parity, the induced polarization is quadrupolar.[9] For the d-block metals, the core atomic orbitals (AOs) are p and the valence orbitals are d, giving an induced polarization that is a dipole. This causes the negative charge to build up trans to the strongly bound ligand, and due to electron−electron repulsion, the trans M−L bond is weakened. In actinide complexes, while the core AOs are p, the

Received: February 6, 2012
Published: May 16, 2012

dx.doi.org/10.1021/ic300273d | Inorg. Chem. 2012, 51, 6190−6199

presence of valence f orbitals causes the polarization to be predominantly quadrupolar. Consequently, the negative charge builds up cis to the strongly bound ligand and an ITI is observed.[9] The polarization explanation is dependent on a deformable core and is consistent with the frequent observation of ITI in larger polarizable metals such as third-row transition[10] and actinide metals.[11] Additionally, ITI has been observed in cobalamins.[12] In uranium complexes, ITI has been observed in inorganic U(VI) oxyhalides[11a,b] and uranyl complexes,[9] prompting various theoretical studies on complexes of the types $[UOX_5]^{n-}$ (X = F, Cl, Br),[13] and $[UOX_4]$ (X = F, Cl, Br).[14] Most of these studies have aimed to determine the validity of Denning's hypothesis on the involvement of the semicore 6p orbitals.

The theoretical description of actinide complexes, especially those with an open-shell f-electron configuration such as those studied here, is difficult due to the combination of pronounced relativistic effects with complicated electron correlation effects. Nevertheless, density-functional methods have generally been found useful in describing actinide compounds in a number of studies; for example, see ref 15. To our knowledge, theoretical investigations on the ITI have so far focused primarily on oxohalides of uranium and other actinide metals.[8a,13,14,16] While common DFT methods using generalized gradient approximation (GGA) functionals appear to provide sound descriptions of actinide complex structures and vibrational frequencies, Shamov et al.[16] have pointed out that hybrid functionals generally lead to higher bond polarity, and consequently these functionals predict a more pronounced ITI in accordance with Denning's electrostatic model.[9] In attempts at a molecular orbital description of ITI, the importance of f orbitals[8a] and 6p semicore states[13] has been stressed.[17] In this contribution, we report structural data on the ITI-exhibiting U(V) coordination complex $[((^{Ad}ArO)_3N)U(NMes)]$, as well as model uranium(V) imide complexes (f^1 electron configuration) obtained using density functional theory with a number of functionals, including GGA, meta-GGA, and hybrid functionals, as well as its synthesis and full spectroscopic characterization. Additionally, syntheses and characterization of the related U(V) trimethylsilylimide complex $[((^{Ad}ArO)_3N)U(NTMS)]$ and U(IV) azide complex $[((^{Ad}ArO)_3N)U(N_3)]$ are presented for comparison.

RESULTS AND DISCUSSION

Synthesis and Molecular Structure of 2. Addition of 1 equiv of a red-brown solution of trivalent $[((^{Ad}ArO)_3N)U]$ (**1**) in diethyl ether to a brown mesityl azide solution in diethyl ether immediately resulted in a dark green solution with evolution of dinitrogen gas. Filtration followed by removal of volatiles yielded a fine dark green powder, which was identified as the U(V) mesitylimide complex $[((^{Ad}ArO)_3N)U(NMes)]$ (**2**) (Scheme 1).

Scheme 1. Synthesis of Pentavalent Uranium Mesitylimide Complex 2

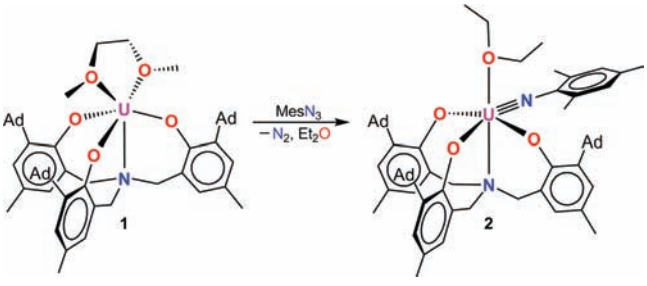

Dark green crystals suitable for XRD analysis were grown from a saturated solution of **2** in ether at room temperature. The molecular structure of **2** features the uranium center in a pseudo-octahedral coordination sphere. Unexpectedly, and in contrast to the case for the uranium trimethylsilylimide complex $[((^{Ad}ArO)_3N)U(NTMS)]$ (**3**) (Figure 4) and previously reported U(V) imide complexes,[18] the mesitylimide ligand is coordinated at the equatorial position cis to the N anchor, while the ether molecule occupies the axial position (Figure 1)

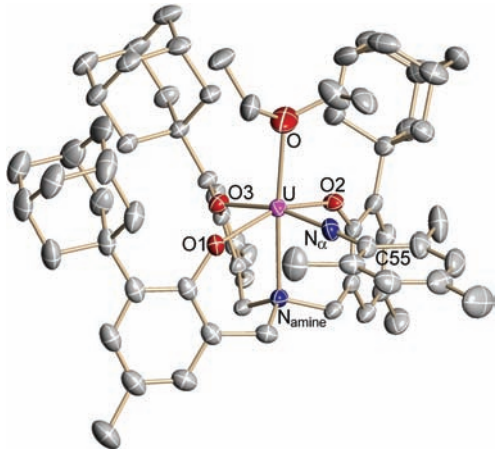

Figure 1. Molecular structure of pentavalent uranium mesitylimide complex **2**. Cocrystallized ether solvent molecules and hydrogen atoms are omitted for clarity. Thermal ellipsoids are at the 50% probability level.

trans to the N anchor. The equatorial coordination of the strongly π-donating $MesN^{2-}$ imido ligand is reflected in a relatively short $U-N_{amine}$ bond length of 2.508(3) Å in complex **2** in comparison to those in the complexes $[((^{Ad}ArO)_3N)U(NTMS)]$ (**3**) (2.630(3) Å) and $[((^{Ad}ArO)_3N)U(N_3)]$ (**4**) (2.631(3) Å), where the $TMSN^{2-}$ ligand of **3** and the N_3^- ligand of **4** occupy the axial position trans to the N anchor and effectively weaken the $U-N_{amine}$ bond. The mesitylimide ligand binds to the uranium center with a $U-N_\alpha-C55$ angle of 177.5(3)°. Although the $MesN^{2-}$ ligand is coordinated equatorially, complex **2** possesses a $U-N_\alpha$ bond length (1.950(3) Å) that is comparable to the $U-N_\alpha$ bond length in **3** (1.943(3) Å), suggesting an equally stable $U-N_\alpha$ bond in **2**. The nearly linear binding angle of the imide fragment and short $U-N_\alpha$ bond length in **2** suggests uranium−nitrogen multiple bonding with a formal U≡NR triple bond. Additionally, the strongly bound mesitylimide ligand exerts an inverse trans influence (ITI) on the uranium−aryloxide bond, U−O3, observed to be the shortest $U-O_{ArO}$ bond within the $[(^{Ad}ArO)_3N)U{\equiv}NMes]$ complex. The U−O3 bond distance is 2.145(2) Å, while the U−O1 and U−O2 bond distances are 2.177(2) and 2.173(2) Å, respectively. Transitioning from a trigonal tris(aryloxide) ligand environment in **1** to a tetragonal tris(aryloxide)imido environment in **2** increases the steric congestion of the adamantyl substituents. Additionally, the ITI in **2** leads to a slightly shorter U−O3 bond, which would also tend to increase steric crowding. Thus, the sterically less advantageous equatorial binding of the strong $MesN^{2-}$ ligand is surmounted by favorable ITI interactions. The correlation between ITI and binding geometry has been studied by Kovács in theoretical studies on the structure and bonding of

dx.doi.org/10.1021/ic300273d | Inorg. Chem. 2012, 51, 6190−6199

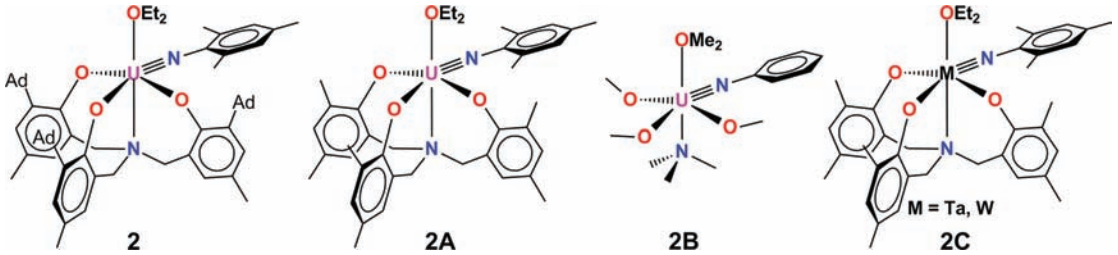

Figure 2. **2** and model complexes **2A**–**C** used in the present density-functional calculations.

$[UOX_4]$ (X = F, Cl, Br, I) complexes.[14] It was determined that $[UOF_4]$ prefers the sterically unfavorable C_{3v} trigonal-bipyramidal arrangement with a linear F–U═O unit over C_{2v} and C_{4v} arrangements due to favorable ITI interactions.[14]

Computational Results on 2. The observed ITI in the molecular structure of **2** is significant but small in magnitude (U–O bond length differences of 0.028 and 0.032 Å) and, as such, may well be influenced by crystal packing and other condensed-phase effects. Nevertheless, the imide ligand is expected to exert a significant classical trans effect in transition-metal chemistry.[8b] To further scrutinize the origins of the observed effect, we present additional results from density functional calculations on **2** and related model complexes (see Figure 2) in the gas phase. The small magnitude of the observed ITI in combination with the size and electronic structure of **2** presents a substantial challenge for the predictive accuracy of present theoretical methods; furthermore, sufficient numerical accuracy (e.g., convergence criteria) of the calculations has to be ensured. As noted in the Computational Details, we present results from several different functionals and two different treatments of relativistic effects and compare the prevalence and magnitude of the calculated ITI in each of these calculations.

An important question is whether the observed ITI in **2** is an electronic effect or a result of the geometry of the chelating tris-aryloxide ligand in **2**. To tackle this question, we have invoked simplified model complexes **2A** and **2B** (see Figure 2) to complement the calculations on **2**. In the first model complex, **2A**, we have merely replaced the bulky adamantyl substituents with methyl groups, thereby reducing the intra-ligand interactions. The second model, **2B**, replaces the chelating, tetradentate ligand by four monodentate ligands. The ligator atoms bound to the U center have been preserved. This drastic simplification allows us to study the effect of the cage structure in **2** and **2A**, which is removed in **2B**. On the other hand, model **2B** introduces additional conformational flexibility, which may hamper the unambiguous identification of an ITI (see below). In the following, we compare computational results from complexes **2**, **2A**, and **2B**.

For the full complex **2**, we have only used the BP GGA-type functional and its dispersion-corrected version BP-D (see Computational Details for more information) for reasons of computational efficiency. Salient bond length parameters for the U–O and U–N bonds are reported in Table 1. As can be seen, the U–O bond lengths in the optimized structure of **2** are very similar to each other, with the maximum difference being 0.018 Å. The U–O bond which is trans to the imide ligand ($U–O_{trans}$), turns out to be *longer* than both $U–O_{cis}$ bonds by less than 0.01 Å (BP/TZVP(ECP) level of theory). At the dispersion-corrected BP-D level, the $U–O_{trans}$ bond is the second shortest among all U–O bonds in **2**.

The theoretical calculations on model complex **2A** are computationally more feasible, which allows us to compare results from a greater variety of density functional methods (Table 1).

Table 1. Salient Calculated Bond Lengths (in Å) in Complexes 2, 2A, and 2B (Figure 2) at Various Levels of Theory[a]

level	$d(U–N_{imide})$	$d(U–O_{trans})$	$d(U–O_{cis,1})$	$d(U–O_{cis,2})$
Compound **2**				
XRD	1.950	**2.145**	2.173	2.177
BP/TZVP(ECP)[b]	1.980	2.183	**2.166**	2.175
BP/TZVP(ECP)[c]	1.982	2.182	**2.164**	2.179
BP-D/TZVP(ECP)[b]	1.962	2.163	**2.158**	2.170
BP-D/TZVP(ECP)[c]	1.962	2.167	**2.157**	2.168
Compound **2A**				
BP/TZVPP(ECP)[b]	1.978	2.160	**2.156**	2.171
BP/TZVPP(ECP)[c]	1.977	2.159	**2.156**	2.172
BP-D/TZVPP(ECP)[b]	1.964	2.163	**2.155**	**2.155**
BP-D/TZVPP(ECP)[c]	1.964	2.161	**2.155**	2.158
PBE/TZVPP(ECP)	1.972	2.160	**2.155**	2.169
PBE-D/TZVPP(ECP)	1.962	2.160	**2.157**	2.160
B97-D/TZVPP(ECP)	1.965	2.167	**2.163**	2.166
TPSS/TZVPP(ECP)	1.975	2.157	**2.151**	2.161
B3LYP/SV(P)(ECP)[b]	1.956	**2.154**	2.157	2.168
B3LYP/SV(P)(ECP)[c]	1.955	**2.152**	2.157	2.171
B3LYP-D/SV(P)(ECP)[b]	1.944	**2.155**	2.158	2.159
B3LYP-D/SV(P)(ECP)[c]	1.943	**2.152**	2.156	2.159
PBE0/SV(P)(ECP)	1.932	**2.132**	2.140	2.150
BP/DZP(ZORA)	*1.967*	***2.166***	*2.170*	*2.175*
BP-D/DZP(ZORA)	1.954	**2.159**	2.168	2.170
Compound **2B**				
BP/TZVPP(ECP)	1.999	2.135	**2.121**	2.122
BP-D/TZVPP(ECP) 1[d]	1.992	**2.113**	2.131	2.134
BP-D/TZVPP(ECP) 2[d]	1.996	2.126	**2.116**	2.124
BP-D/TZVPP(ECP) 3[d]	1.991	2.126	**2.120**	2.126
TPSS/TZVPP(ECP)	1.997	2.129	**2.117**	**2.117**
TPSSh/TZVPP(ECP)	1.981	2.116	**2.109**	2.110
B3LYP/TZVPP(ECP) 1[e]	1.979	2.128	**2.123**	2.126
B3LYP/TZVPP(ECP) 2[e]	1.977	**2.113**	2.128	2.134
B3LYP-D/TZVPP(ECP)	1.977	**2.111**	2.122	2.131
PBE0/TZVPP(ECP)	1.957	2.106	**2.105**	2.106
BP-D/DZP(ZORA)	1.994	**2.119**	2.136	2.138
BP/DZP(ZORA)	1.998	**2.119**	2.143	2.144

[a]The shortest U–O bonds are given in boldface type. [b,c]Different conformers corresponding to the disorder of the OEt_2 ligand in the X-ray structure. [d]1, 2, and 3 refer to three different conformers found at the BP-D level for complex **2B**; see the main text for details. [e]1 and 2 refer to two different conformers found at the B3LYP level.

In general, we observe similarly small differences in the $U–O_{ArO}$ bond lengths like those observed for **2** at all computational levels. The optimized geometries obtained using the GGA-type functionals (such as BP, PBE) do not confirm the results obtained for the parent compound **2**; i.e., the computed $U–O_{trans}$ bond distances are slightly larger than those of $U–O_{cis}$. However,

dx.doi.org/10.1021/ic300273d | Inorg. Chem. 2012, 51, 6190–6199

from Table 1 one can also see that the hybrid functionals (B3LYP, B3LYP-D, and PBE0), unlike the GGAs and meta-GGAs, find the U−O_{trans} bond length as the shortest among all three U−O bonds. Hence, these functionals clearly suggest the presence of an ITI in **2A** (the higher tendency of hybrid functionals as compared to GGA functionals in favor of a more pronounced ITI has been observed before).[16] A comparison of the ZORA calculations (ADF program) with the ECP calculations (Turbomole program) at the BP density functional level suggests that the treatment of relativistic effects can also have an influence on whether an ITI is predicted or not: the BP/ZORA calculations do predict the U−O_{trans} bond as the shortest, while with the BP/ECP method, U−O_{trans} is shorter than one of the U−O_{cis} bonds but longer than the other. It should be noted, however, that the predicted bond length difference is on the order of only 0.01 Å and hence is smaller than the bond length differences observed in the X-ray crystal structure analysis of **2**. Furthermore, details in the implementation of the two DFT programs used may also affect the results to some extent.

Finally, we turn to the computational results for the model complex **2B**, which replaces the chelating ligand in **2** by four monodentate ligands. This model was envisaged to remove any constraints due to the specific structure of the ligand in **2**, which may allow a better study of the electronic part of the ITI. On first observation, all calculated bond lengths are shorter than those in **2** and **2A**, presumably due to reduced inter-ligand repulsion. Second, most calculations which employ an effective core potential (ECP) do not predict the U−O_{trans} bond as the shortest bond (Table 1). This includes calculations done with hybrid functionals. Rather, the U−O_{trans} bond is longer by approximately 0.01 Å compared to the shortest U−O_{cis} bond for most levels. Moreover, a number of test calculations at the BP-D/TZVPP(ECP) have shown (see Table 1 and the Supporting Information for details) that the prediction of an ITI or not depends delicately on the conformation of the local minimum found at a given level of theory. For instance, at the BP-D/TZVPP(ECP) level (using strict optimization criteria; see the Computational Details and the Supporting Information), we find three different conformers of model complex **2B** (see the Supporting Information for structures), two of which formally do not show an ITI, while the third does show U−O_{trans} as the shortest bond among all. Remarkably, all three structures have the same energy within only 0.3 kJ/mol, which is far below the accuracy of the method. Similarly, two closely related conformers have been found at the B3LYP level (Table 1). This shows that the increased conformational flexibility of model **2B** hampers an unambiguous analysis of the ITI. Nevertheless, we note that, in contrast to the ECP-based methods, a clear ITI is predicted at the BP/ZORA level (Table 1). The presence of other conformers which may or may not show an ITI has not been tested at this level, however.

In summary, the ITI in **2** and model complexes **2A** and **2B** can be characterized by the relative shortness of the U−O_{trans} bond compared to the other two U−O_{cis} bonds. Taking such a strict definition of the ITI as a basis, the present computations on the full system **2** do not unambiguously show U−O_{trans} as the shortest bond. Hybrid functionals do consistently predict a small ITI for **2A**, although the effect of basis set size needs further investigation here. For **2B**, the observation of an ITI or not appears to be connected to the conformation adopted by the complex. For the BP/TZVPP(ECP) level, at least three isoenergetic conformers of **2B** have been found, one of which shows a clear ITI. Moreover, the BP/ZORA method predicts a pronounced ITI in **2B**.

Considering that the imide ligand is expected to exert a strong classical trans influence in transition metal coordination chemistry (M−L_{trans} lengthening as large as 0.32 Å for W(VI) complexes),[8b] one would actually anticipate a significantly longer U−O_{trans} bond length in comparison to the U−O_{cis} bond lengths. This is generally not observed in the calculations, however, and the fact that the elongation of U−O_{trans} compared to U−O_{cis} is actually very small (less than 0.01 Å) may be taken as an indication for the presence of an ITI.

To illustrate this argument, in Table 2 we show results from additional calculations on complexes **2C** (Figure 2),

Table 2. Salient Calculated Bond Lengths (in Å) and M−O Bond Length Differences in Model Complexes 2A (M = U) and 2C (M = Ta, W) at Several Levels of Theory and Using the SV(P) Basis Set with ECP on Ta, W, or U[a]

level	d(M−N_{imide})	d(M−O_{trans})	d(M−$O_{cis,1}$)	d(M−$O_{cis,2}$)	Δ[b]
		M = Ta			
BP	1.861	2.133	**1.998**	2.005	0.128
BP-D	1.850	2.129	**1.999**	2.003	0.126
B3LYP	1.847	2.131	**1.993**	2.000	0.131
B3LYP-D	1.837	2.129	**1.995**	1.996	0.133
		M = W			
BP	1.818	2.084	**2.049**	2.050	0.034
BP-D	1.808	2.087	**2.033**	2.044	0.043
B3LYP	1.803	2.085	**2.043**	2.047	0.038
B3LYP-D	1.794	2.088	**2.029**	2.039	0.049
		M = U			
BP	1.978	2.162	**2.155**	2.169	−0.007
BP-D	1.964	2.161	**2.155**	2.156	0.005
B3LYP	1.956	**2.154**	2.157	2.168	−0.014
B3LYP-D	1.944	**2.155**	2.158	2.159	−0.004

[a]Cf. Computational Details; the shortest M−O bonds are given in boldface type. [b]Δ = difference between d(M−O_{trans}) and d(M−$O_{cis,2}$).

which bear transition-metal centers Ta and W rather than U in **2A.** Table 2 shows that in both the Ta and W complexes the M−O_{trans} distance is longer than both M−O_{cis} distances. In the U complex **2A**, however, the U−O_{trans} and the longest U−O_{cis} bonds are similar within approximately 0.01 Å. These data suggest that the arylimide ligand exerts a normal trans influence in **2C** for the transition metals Ta and W. Clearly, the same classical trans influence is not observed for **2A**. It is furthermore noteworthy that the normal trans influence in **2C** is larger for M = Ta (d^0 electron configuration) than for M = W (d^1 electron configuration).

Finally, it should be noted that the differences in bond lengths predicted by most of the calculations shown here are small. The magnitude of the effect constitutes a significant challenge for present-day density-functional calculations on large actinide complexes.

Magnetism and Electronic Absorption of 2. The VT SQUID magnetization data of **2** shows a narrow magnetic moment range of 1.0−1.68 μ_B in the temperature range between 5 and 300 K (Figure 3, top). The decreased magnetic moment of 1.68 μ_B in comparison to the calculated value of 2.54 μ_B[19] for a U(V) f^1 complex at 300 K can be attributed to increased covalency in the U≡NMes unit, which quenches spin−orbit coupling and results in a lower observed effective magnetic moment.

dx.doi.org/10.1021/ic300273d | Inorg. Chem. 2012, 51, 6190−6199

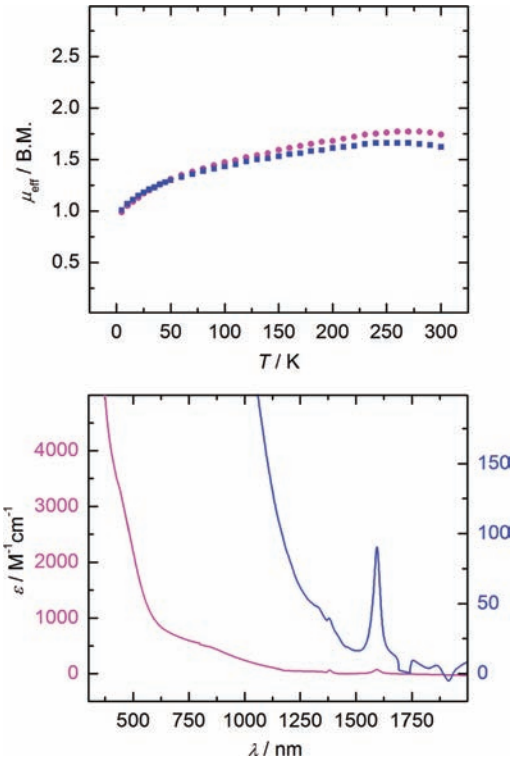

Figure 3. Temperature-dependent SQUID magnetization data of two independently synthesized samples of **2** (at 1 T) plotted as a function of magnetic moment (μ_{eff}) vs temperature (T) (top). The electronic absorption spectrum of **2** is recorded in tetrahydrofuran (bottom).

The intense dark green color of complex **2** is reflected in the electronic absorption spectrum, which features two very broad, unresolved LMCT bands in the UV and visible region with extinction coefficients ranging from ~500 to 3000 M^{-1} cm^{-1} (Figure 3; bottom, magenta). Along with these LMCT transitions, weak f–f transitions are also observed in the near-IR region ($\varepsilon \approx 50–100$ $M^{-1}cm^{-1}$). Both VT SQUID magnetization data and electronic absorption data support an oxidation state assignment of +5 for the uranium center.

Synthesis and Molecular Structure of 3. Treating a red-brown solution of **1** in diethyl ether (Et_2O) with a solution of azidotrimethylsilane in ether results in a red-orange solution with concomitant release of N_2 gas. The reaction solution was filtered, and the volatiles were removed to yield red-orange solids, which were identified as the U(V) trimethylsilylimide complex $[((^{Ad}ArO)_3N)U(NTMS)]$ (**3**) (Scheme 2, top).

Dark orange single crystals of **3**, suitable for XRD analysis, were grown from a saturated solution of **3** in ether at room temperature. The molecular structure of **3** displays the uranium center in a pseudo-octahedral environment coordinated by the $TMSN^{2-}$ ligand in the axial position trans to the N anchor, and by an ether molecule in the equatorial position cis to the imide group (Figure 4). The $U–N_{amine}$ distance in **3** of 2.630(3) Å is significantly longer than that in **2**, while the average $U–O_{ArO}$ distance of 2.154 Å is more comparable to that in **2** (Table 3). The combination of an almost linearly bound imide ligand ($\angle U–N_\alpha–Si = 175.7(2)°$) and short $U–N_\alpha$ distance (1.943(3) Å) in **3** suggests $U–N_\alpha$ multiple bonding with a formal U≡NR triple bond. Consequently, the $U–N_\alpha$ distance is relatively short compared to those of the previously reported trimethylsilylimide complexes $[((^{t\text{-}Bu}ArO)_3tacn)U(NTMS)]$ (1.985(5) Å)[20] and $[((^{Ad}ArO)_3tacn)U(NTMS)]$ (2.122(2) Å).[21] As a result,

Scheme 2. Syntheses of U(V) Trimethylsilylimide Complex 3 and U(IV) Azide Complex 4

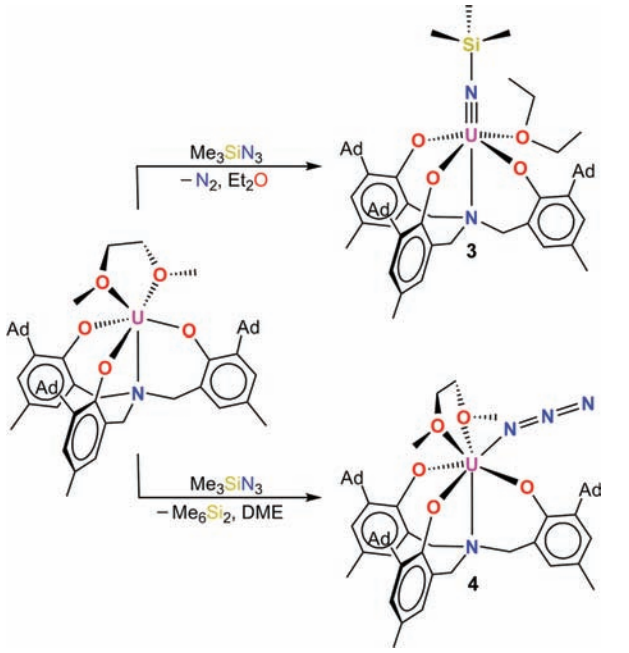

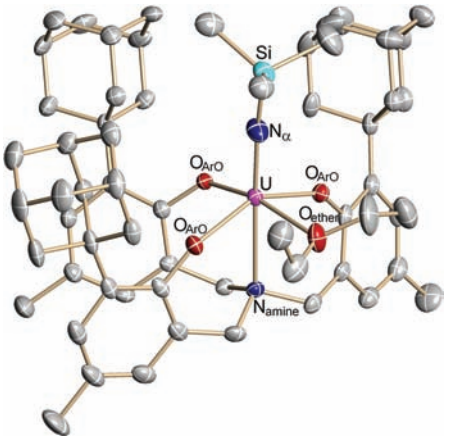

Figure 4. Molecular structure of pentavalent uranium trimethylsilylimide complex **3**. Cocrystallized ether solvent molecules and hydrogen atoms are omitted for clarity. Thermal ellipsoids are at the 50% probability level.

Table 3. Selected Bond Distances (Å) and Angles (deg) for 2–4

structural parameters	2	3	4
$U–N_{amine}$	2.508(3)	2.630(3)	2.631(3)
$U–O_{ArO}$ (av)	2.165	2.154	2.168
$U–O_{DME}$ (av, **4**), $U–O_{ether}$ (**2**, **3**)	2.435(3)	2.563(3)	2.613
$U–N_\alpha$	1.950(3)	1.943(3)	2.422(4)
$N_\alpha–N_\beta$			1.101(5)
$N_\beta–N_\gamma$			1.189(6)
$N_\alpha–Si$		1.725(3)	
$N_\alpha–C55$	1.391(5)		
$\angle N_\alpha–N_\beta–N_\gamma$			177.6(5)
$\angle U–N_\alpha–N_\beta$			151.8(3)
$\angle U–N_\alpha–Si$		175.7(2)	
$\angle U–N_\alpha–C55$	177.5(3)		

dx.doi.org/10.1021/ic300273d | Inorg. Chem. 2012, 51, 6190–6199

the N_α–Si bond length of 1.725(3) Å is longer compared to those of complexes [(($^{t\text{-Bu}}$ArO)$_3$tacn)U(NTMS)] (1.713(5) Å)[20] and [((^{Ad}ArO)$_3$tacn)U(NTMS)] (1.623(2) Å).[21] In principle, cleavage of the N_α–Si bond would yield the uranium terminal nitride species, and the significantly weakened N_α–Si bond is a promising observation. Of interest to note is the ether molecule coordinated cis to the $TMSN^{2-}$ ligand in the equatorial position. In addition to demonstrating the flexibility of the N-anchored tris-aryloxide ligand, the weakly bound ether ($U–O_{ether}$ = 2.563(3) Å) can be readily displaced, thus leaving a vacant site for additional incoming substrates. The flexibility of the ligand in trivalent complex **1** could potentially lead to reactivity toward small molecules different from that previously observed in sterically crowded U(III) complexes [((^{R}ArO)$_3$tacn)U] (R = *t*-Bu, Ad), where only coordination at the seventh axial position is possible.

Magnetism and Electronic Absorption of 3. The VT SQUID magnetization data of **3** display effective magnetic moment values ranging from 0.90 μ_B at 2 K to 1.57 μ_B at 300 K (Figure 5, top). The μ_{eff} value of 1.57 μ_B is lower than the

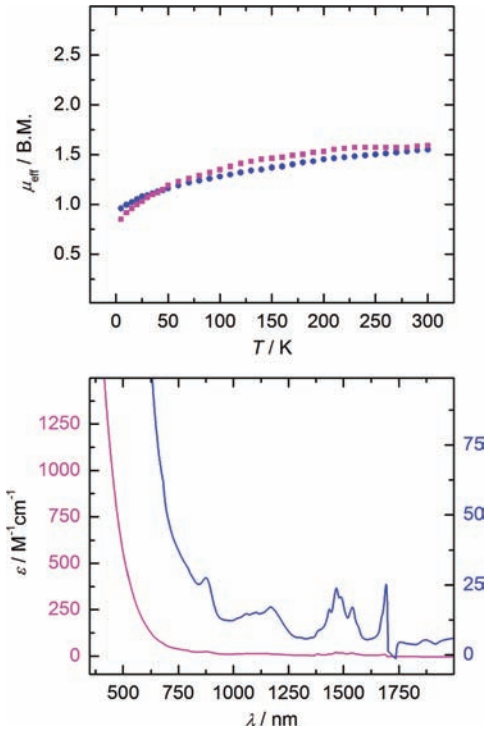

Figure 5. Temperature-dependent SQUID magnetization data of two independently synthesized samples of **3** (at 1 T) plotted as a function of magnetic moment (μ_{eff}) vs temperature (T) (top). The electronic absorption spectrum of **3** is recorded in tetrahydrofuran (bottom).

calculated effective magnetic moment at room temperature for a U(V) f^1 complex (2.54 μ_B).[22] Reminiscent of complex **2**, the increased covalency in the U–NTMS unit, indicated by the relatively short $U–N_\alpha$ bond distance of 1.943(3) Å, reduces the observed effective magnetic moment.

The intense colors of uranium complexes can result from either a Laporte-allowed f–d or ligand-to-metal charge transfer transitions. The $5f^3$ to $5f^26d^1$ transition is typically observed for trivalent uranium complexes. Electronic absorption spectra of pentavalent uranium complexes commonly show weak Laporte-forbidden f–f transitions over the entire spectral UV/vis/near-IR range, in addition to LMCT transitions in the UV–vis region. The electronic absorption spectrum of **3** shows intense, unresolved charge-transfer bands over the entire visible part of the absorption spectrum (Figure 5; bottom, magenta). Additionally, the typical Laporte-forbidden f–f transitions are observed in the visible and near-IR region (Figure 5; bottom, blue). The VT SQUID magnetization and electronic absorption data support a U(V) center in uranium imide complex **3**.

Synthesis and Molecular Structure of 4. We have shown earlier that the reaction of U(III) complexes with azidotrimethylsilane can—depending on reaction conditions—result in U(V) imide and U(IV) azide formation.[18a] Accordingly, treatment of a red-brown solution of the trivalent uranium complex [((^{Ad}ArO)$_3$N)U] (**1**) in 1,2-dimethoxyethane (DME) with 1 equiv of azidotrimethylsilane, instead of diethyl ether, immediately results in a yellow-orange solution. Over several hours, formation of a green precipitate is observed. The green product was collected by filtration and identified as the U(IV) azide complex [((^{Ad}ArO)$_3$N)U(N$_3$)] (**4**) (Scheme 2, bottom). Cooling a saturated solution of [((^{Ad}ArO)$_3$N)U(N$_3$)] (**4**) in DME at −35 °C produced single crystals suitable for XRD analysis. The molecular structure of **4** contains the tetradentate ligand in addition to an η^1-coordinated azide ligand and a κ^2-bound DME solvent molecule coordinated to the uranium center (Figure 6). The $U–N_{amine}$ and average $U–O_{ArO}$ distances in **4** of

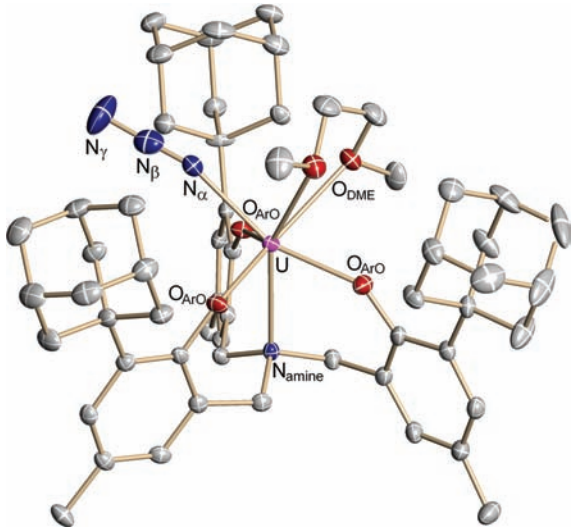

Figure 6. Molecular structure of U(IV) azide complex **4**. Cocrystallized DME solvent molecules and hydrogen atoms are omitted for clarity. Thermal ellipsoids are at the 50% probability level.

2.631(3) and 2.168 Å, respectively, are comparable to those of the starting complex **1** (2.622(4), 2.222 Å). The nearly linear azide unit, with an $N_\alpha–N_\beta–N_\gamma$ angle measuring 177.6(5)°, coordinates to the uranium center at a $U–N_\alpha–N_\beta$ angle of 151.8(3)°. This $U–N_\alpha–N_\beta$ angle is comparable to the metal–azide angles observed for other uranium(IV) azide species.[3d,20,21,23] Complex **4** has a much shorter $U–N_\alpha$ bond of 2.422(4) Å compared to that in [(($^{t\text{-Bu}}$ArO)$_3$tacn)U(N$_3$)], which exhibits a $U–N_\alpha$ bond distance of 2.564(12) Å. The $N_\alpha–N_\beta$ and $N_\beta–N_\gamma$ bond lengths of 1.101(5) and 1.189(6) Å in **4** are inequivalent and unusual, in that the $N_\alpha–N_\beta$ bond is significantly shorter than the $N_\beta–N_\gamma$ bond. This is not in agreement with the resonance structures of a metal-coordinated azide ligand (M–N=N=N ↔ M–N–N≡N) and, thus, is attributed to a crystallographic disorder of the

dx.doi.org/10.1021/ic300273d | Inorg. Chem. 2012, 51, 6190–6199

azide fragment in the crystal structure. Attempts at modeling the disorder did not lead to satisfactory refinement parameters.

Magnetism and Electronic Absorption of 4. Unlike U(V) f^1 complexes, U(IV) f^2 complexes exhibit very low effective magnetic moments at low temperatures due to their nonmagnetic singlet ground states. The effective magnetic moment (μ_{eff}) of complex **4** at 2 K of 0.34 μ_B is within the usual range of 0.4−0.8 μ_B (2−5 K). However, the room-temperature magnetic moment of **4** is significantly lower than is typically observed (2.14 μ_B at 300 K) (Figure 7, top). The significantly lower magnetic moment

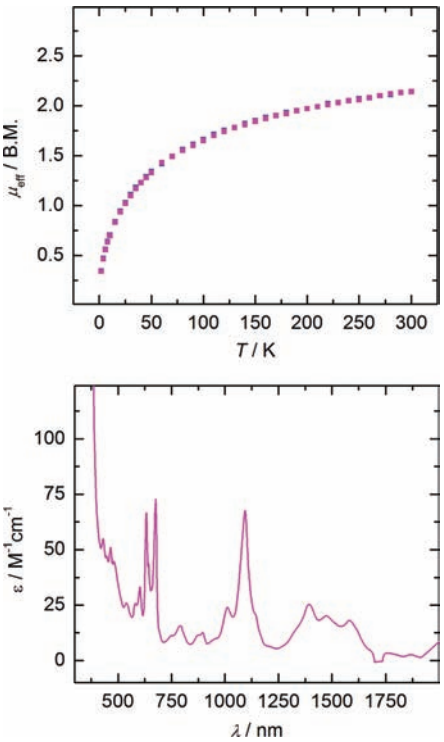

Figure 7. Temperature-dependent SQUID magnetization data of two independently synthesized samples of **4** (at 1 T) plotted as a function of magnetic moment (μ_{eff}) vs temperature (T) (top). The electronic absorption spectrum of **4** is recorded in tetrahydrofuran (bottom).

observed for **4**, as compared to that of $[((^{Ad}ArO)_3tacn)U(N_3)]$ (0.69 μ_B, 5 K; 2.87 μ_B, 300 K), could be attributed to covalency within the U−azide unit. The increased covalency is supported through the linear coordination, which allows for better π bonding and, consequently, results in the observed atypically short U−N bond. Although the effective magnetic moment at room temperature is unexpectedly low, the dependence of the magnetic moment on temperature is commonly observed for U(IV) species of similar ligand systems.[18a] Unfortunately, magnetic data, even in a descriptive fashion, are scarce in uranium coordination chemistry. A more detailed collaborative study is underway.

Aside from exhibiting an unusual room-temperature magnetic moment, the electronic absorption data of **4** confirm a tetravalent uranium center. The pale green color of **4** is an effective visual indicator that no charge-transfer or f−d transitions will be observed. Accordingly, the electronic absorption spectrum of **4** features only weak bands ($\varepsilon \approx 10-75$ M^{-1} cm^{-1}) in the vis/near-IR region arising from Laporte-forbidden f−f transitions (Figure 7, bottom). These f−f transitions are similarly observed for the U(IV) azide complexes of the $[((^{R}ArO)_3tacn)U(N_3)]$ type.[20,21]

CONCLUSION

With the purpose of studying uranium−ligand multiple bonds and ultimately isolating a uranium terminal nitride species, we set out to obtain uranium imide and azide complexes with our newly developed, single N-anchored tris(aryloxide) U(III) system, namely $[(^{Ad}ArO)_3N)U]$ (**1**). Like the previously developed six-coordinate tacn-based tris(aryloxide) uranium complex, four-coordinate **1** is electron-rich; however, the latter is significantly more coordinatively unsaturated. Additionally, the $(^{Ad}ArO)_3N^{3-}$ chelator exhibits remarkable flexibility, supporting uranium complexes in both trigonal and tetragonal ligand environments. Activation of mesityl azide by **1** resulted in the isolation of the U(V) mesitylimide complex **2**. The mesitylimide ligand exhibits an inverse trans influence, an unusual observation that is not well-documented for non-actinyl and non-halide actinide complexes. Complex **2** is also the first example of a U(V) to exhibit this phenomenon. To further corroborate this effect, we have performed additional density functional calculations on **2** and simplified model complexes. The magnitude and presence of the ITI predicted depends on the density functional method used. Our calculations suggest that effective core potentials in combination with hybrid functionals show a greater tendency to predict an ITI in comparison to GGA and meta-GGA functionals, as does the ZORA method in combination with the BP functional. The ITI predicted is small, however, and may furthermore delicately depend on slight conformational changes in the molecular structure of the complex. Taking into account that, in classical transition-metal coordination chemistry, the imide ligand is usually exerting a strong, classical trans influence, the present calculations suggest that the inverse trans influence observed in **2** is not due to crystal-packing effects but is rather intrinsic. The activation of azidotrimethylsilane by **1** resulted in isolation of U(V) trimethylsilylimide complex **3** and U(IV) azide complex **4**. The U(V) trimethylsilylimide complex **3** offers a vacant cis position for further chemistry, a characteristic not observed in complexes of previous tacn-based ligand systems. Overall, the reactivity of **1** with organic azides have produced compounds that are markedly different from those of previous uranium complexes, employing tacn-based ligands. The unusual characteristics exhibited by complexes **2** and **3** are promising. Investigations on the further reactivity of these compounds are currently underway.

EXPERIMENTAL SECTION

General Methods. All experiments were performed under a dry nitrogen atmosphere using standard Schlenk techniques or an MBraun inert-gas glovebox. Solvents were purified using a two-column solid-state purification system (Glasscontour System, Irvine, CA) and transferred to the glovebox without exposure to air.

Spectroscopic Methods. Magnetization data of crystalline powdered samples (20−30 mg) were recorded with a SQUID magnetometer (Quantum Design) at 10 kOe (2−300 K for **4**) and (5−300 K for **2** and **3**). Values of the magnetic susceptibility were corrected for the underlying diamagnetic increment (χ_{dia} = -717.82×10^{-6} cm^3 mol^{-1} (**2**), -676.98×10^{-6} cm^3 mol^{-1} (**3**), -647.71×10^{-6} cm^3 mol^{-1} (**4**)) by using tabulated Pascal constants and the effect of the blank sample holders (gelatin capsule/straw). Samples used for magnetization measurements were recrystallized multiple times and checked for chemical composition and purity by elemental analysis (C, H, and N) and ^{1}H NMR spectroscopy. Data reproducibility was also carefully checked on independently synthesized samples.

^{1}H NMR spectra were recorded on JEOL 270 and 400 MHz instruments operating at the respective frequencies of 269.714 and 400.178 MHz with a probe temperature of 23 °C in THF-d_8. Chemical

dx.doi.org/10.1021/ic300273d | Inorg. Chem. 2012, 51, 6190−6199

shifts were referenced to protio solvent impurities (δ 1.73, 3.58 (THF-d_8)) and are reported in parts per million.

Electronic absorption spectra were recorded from 200 to 2000 nm (Shimadzu (UV-3101PC)) in the indicated solvent.

Results from elemental analysis were obtained from the Analytical Laboratories at the Friedrich-Alexander-University Erlangen-Nuremberg (Erlangen, Germany) on a Euro EA 3000 instrument.

Starting Materials. The precursor complexes $[(THF)_4UI_3]$ and $[U(N(SiMe_3)_2)_3]$ were prepared as described by Clark et al.[24a−c] The trivalent uranium complex $[((^{Ad}ArO)_3N)U]$ (**1**) was prepared according to published procedures.[24d] Uranium turnings were purchased from Oak Ridge National Laboratory (ORNL) and activated according to literature procedures.[24a−c] Azidotrimethylsilane (95%) was purchased from Sigma-Aldrich and used as received. Mesityl azide was synthesized according to a literature procedure.[25] Anhydrous 1,2-dimethoxyethane (99.5%) was purchased from Aldrich and further dried by distilling over sodium benzophenone.

Synthesis of $[((^{Ad}ArO)_3N)U(NMes)]$ (2). A red-brown suspension of complex **1** (100 mg, 0.090 mmol) in diethyl ether (∼6 mL) was added dropwise to a stirred solution of mesityl azide (17.5 μL, 17.5 mg, 0.109 mmol) in diethyl ether (∼2 mL). Immediately, the reaction solution became dark green and dinitrogen gas evolution was observed. The reaction mixture was stirred for 2 h and then filtered through a glass filter paper. Removal of volatiles yielded dark green solids of **2** (yield 82 mg, 0.067 mmol, 74%). ^{1}H NMR (290 MHz, THF-d_8, 20 °C): δ 18.2 (br. s, 3H, $\Delta\nu_{1/2}$ = 38 Hz), 17.8 (br s, 3H, $\Delta\nu_{1/2}$ = 65 Hz), 11.8 (v br s, 6H, $\Delta\nu_{1/2}$ = 212 Hz), 11.4 (br s, 3H, $\Delta\nu_{1/2}$ = 49 Hz), 6.30 (s, 3H, $\Delta\nu_{1/2}$ = 13 Hz), 3.27 (s, 2H, $\Delta\nu_{1/2}$ = 0.6 Hz), 2.70 (s, 9H, $\Delta\nu_{1/2}$ = 6 Hz), 2.31 (s, 3H, $\Delta\nu_{1/2}$ = 2.6 Hz), 0.26 (s, 9H, $\Delta\nu_{1/2}$ = 17 Hz), −0.23 (s, 9H, $\Delta\nu_{1/2}$ = 15 Hz), −0.60 (br. s, 9H, $\Delta\nu_{1/2}$ = 30 Hz), −4.82 (v. br. s, 18H, $\Delta\nu_{1/2}$ = 95 Hz. Anal. Calcd for **2**: C, 65.83; H, 7.17; N, 2.29. Found: C, 66.03; H, 7.12; N, 2.47.

Synthesis of $[((^{Ad}ArO)_3N)U(NTMS)]$ (3). A red-brown suspension of complex **1** (100 mg, 0.090 mmol) in diethyl ether (∼6 mL) was added dropwise to a solution of azidotrimethylsilane (15 μL, 12.4 mg, 0.107 mmol) in diethyl ether (∼2 mL). Nitrogen evolution was observed, along with an immediate solution color change to red-orange. The reaction was allowed to proceed for 2 h. The solution was filtered through a glass filter paper, and the volatiles were removed to yield red-orange solids of **3** (yield 85 mg, 0.072 mmol, 80%). ^{1}H NMR (290 MHz, THF-d_8, 20 °C): δ 5.73 (v br s, 12H, $\Delta\nu_{1/2}$ = 91 Hz), 2.84 (m, 3H, $\Delta\nu_{1/2}$ = 8.5 Hz), 2.56 (m, 3H, $\Delta\nu_{1/2}$ = 10 Hz), 0.37 (br s, 12H, $\Delta\nu_{1/2}$ = 29 Hz), 0.15 (br s, 18H, $\Delta\nu_{1/2}$ = 20 Hz), −0.12 (v br s, 12H, $\Delta\nu_{1/2}$ = 187 Hz), −1.21 (br s, 15H, $\Delta\nu_{1/2}$ = 39 Hz). Anal. Calcd for **3**: C, 62.28; H, 7.28; N, 2.38. Found: C, 62.49; H, 7.06; N, 2.54.

Synthesis of $[((^{Ad}ArO)_3N)U(N_3)]$ (4). *Method 1.* Azidotrimethylsilane (15 μL, 12.4 mg, 0.107 mmol) diluted in DME (∼2 mL) was added dropwise to a stirred red-brown suspension of complex **1** (100 mg, 0.090 mmol) in DME (∼6 mL). Immediately, all solids were solvated and the solution turned yellow-orange. The reaction was allowed to proceed for 10 h, after which a green precipitate formed. The reaction mixture was concentrated to one-third the volume and placed in a −35 °C freezer. After a few hours, the green precipitate was filtered cold and dried under vacuum, yielding **4** as a fine green powder, in low yields.

Method 2. A more superior method for preparing complex **4** involves dissolving $[((^{Ad}ArO)_3N)U(Cl)]$ (200 mg, 0.18 mmol) in 6 mL of benzene and adding NaN_3 (23 mg, 0.36 mmol) with stirring. The reaction mixture was stirred overnight, after which it was filtered through a glass paper filter inside a pipet. All volatiles were removed from the filtrate to give $[((^{Ad}ArO)_3N)U(N_3)]$ (**4**) as a light green powder. Green prism-shaped crystals of **4** were obtained from DME diffusion into a concentrated solution of benzene (yield 130 mg, 0.11 mmol, 64%). ^{1}H NMR (290 MHz, THF-d_8, 20 °C): δ 10.2 (s, 18H, $\Delta\nu_{1/2}$ = 15 Hz), 3.74 (s, 9H, $\Delta\nu_{1/2}$ = 13 Hz), 3.42 (s, 6H, $\Delta\nu_{1/2}$ = 2.6 Hz), 3.27 (s, 9H, $\Delta\nu_{1/2}$ = 2.6 Hz), 2.88 (s, 3H, $\Delta\nu_{1/2}$ = 13 Hz), 2.84 (s, 6H, $\Delta\nu_{1/2}$ = 16 Hz), 2.56 (s, 6H, $\Delta\nu_{1/2}$ = 13 Hz), 2.52 (s, 3H, $\Delta\nu_{1/2}$ = 15 Hz), 2.37 (s, 3H, $\Delta\nu_{1/2}$ = 8.5 Hz), 2.14 (s, 9H, $\Delta\nu_{1/2}$ = 5.3 Hz), −17.7 (s, 4H, $\Delta\nu_{1/2}$ = 59 Hz). Anal. Calcd for **4**: C, 60.72; H, 6.68; N, 4.88. Found: C, 61.00; H, 6.97; N, 4.41.

Computational Details. Density functional calculations were performed using the Turbomole[26] and the ADF[27] program packages. The geometries of **2** and model complexes **2A−C** were optimized using various exchange-correlation functionals at the generalized gradient approximation (GGA), meta-GGA, and hybrid levels. In particular, the BP,[28] PBE,[29] TPSS,[30] B97D,[31] TPSSh,[32] B3LYP,[33] and PBE0[34] functionals were used. Strict geometry convergence criteria (energy change below 10^{-6} au and gradient norm below 10^{-4} au) in combination with fine quadrature grids (grid m5 for Turbomole, integration accuracy parameter of at least 6 for ADF) were applied to ensure convergence of bond lengths to better than 0.01 Å within a given functional/basis set combination. The geometry optimizations were generally started from the heavy-atom positions provided by the X-ray crystallographic structure. Basis sets of polarized triple-ζ quality (TZVPP) or double-ζ basis sets with polarization functions on non-hydrogen atoms (SV(P)) were used for Turbomole, as indicated in the text.[35] These basis sets in Turbomole imply a scalar-relativistic Stuttgart small-core (60 core electron) effective core potential (ECP) on U, Ta, and W[36] and no pseudopotentials on the other atoms. The multipole-accelerated resolution of the identity approximation for the Coulomb energy was used in the Turbomole calculations.[35a,37] For the ADF calculations, relativistic effects were treated using the zero-order regular approximation (ZORA) Hamiltonian in its scalar-relativistic version.[38] Spin−orbit coupling effects in the collinear and noncollinear spin approximation were taken into account in some test cases and were found to have minor impact on the geometries; see the Supporting Information for details. Various Slater-type basis sets of triple-ζ (TZ2P) and double-ζ (DZP) quality from the ADF-ZORA library and small frozen cores were employed. DZP implies a triple-ζ basis set with one polarization function on U and a double-ζ basis set with polarization function on the other atoms, while the label TZ2P implies a triple-ζ basis set with two sets of polarization functions on U, triple-ζ basis sets with one set of polarization functions on the ligator atoms N and O, and a double-ζ basis set with polarization function on the other atoms. Long-range van der Waals dispersion corrections according to Grimme (DFT-D2)[31] were applied (both Turbomole and ADF), as indicated in the text; corresponding calculations are labeled by appending "-D" to the functional acronym (e.g., BP-D for dispersion-augmented BP calculations).

Crystallographic Details for 2. Dark green block-shaped crystals, grown from a saturated solution of **2** in diethyl ether at room temperature, were coated with isobutylene oil on a microscope slide. A crystal of approximate dimensions 0.18 × 0.15 × 0.13 mm^3 was selected and mounted on a nylon loop. A total of 193 275 reflections ($-30 \le h \le 30$, $-17 \le k \le 24$, $-32 \le l \le 33$) were collected at T = 100(2) K in the θ range from 2.77 to 27.88°, 13 308 of which were unique (R_{int} = 0.0510) and 9628 were observed ($I > 2\sigma(I)$) on a Bruker Kappa APEX2 Duo diffractometer equipped with an Incoatec IμS microsource and focusing Montel optics (QUAZAR) using Mo Kα radiation (λ = 0.710 73 Å). The structure was solved by direct methods and refined by full-matrix least-squares procedures on F^2 (SHELXTL NT 6.12, Bruker AXS, Inc., 2002). All non-hydrogen atoms were refined anisotropically. Hydrogen atoms were placed in calculated idealized positions. The coordinating diethyl ether molecule is disordered. Two orientations of one of the ethyl groups were refined with occupancies of 55(2)% for C66, C67 and 45(2)% for C66A, C67A. The residual peak and hole electron densities were 2.362 and −0.972 e Å^{-3}. The absorption coefficient was 2.961 mm^{-1}. The least-squares refinement converged normally with residuals of R1 = 0.0574, wR2 = 0.0898, and GOF = 1.112 (all data). Crystal data: $C_{67}H_{87}N_2O_4U$, orthorhombic, space group *Pbca*, a = 23.411(3) Å, b = 18.614(3) Å, c = 25.602(4) Å, V = 11 156(3) Å^3, Z = 8, ρ_{calcd} = 1.456 Mg/m^3, $F(000)$ = 5016, R1(F) = 0.0309, wR2(F^2) = 0.0727 ($I > 2\sigma(I)$). CCDC reference number: CCDC 862723.

Crystallographic Details for 3. Brown-orange block-shaped crystals, grown from a saturated solution of **3** in diethyl ether at room temperature, were coated with isobutylene oil on a microscope slide. A crystal of approximate dimensions 0.21 × 0.20 × 0.17 mm^3 was selected and mounted on a nylon loop. A total of 77 821 reflections ($-38 \le h \le 38$, $-23 \le k \le 23$, $-30 \le l \le 30$) were collected at T = 150(2) K in the θ range from 3.40 to 27.10°, 12 449 of which were

dx.doi.org/10.1021/ic300273d | *Inorg. Chem.* 2012, 51, 6190−6199

unique (R_{int} = 0.0789) and 8812 were observed ($I > 2\sigma(I)$) on a Bruker-Nonius KappaCCD diffractometer using Mo Kα radiation (λ = 0.710 73 Å, graphite monochromator). The structure was solved by direct methods and refined by full-matrix least-squares procedures on F^2 (SHELXTL NT 6.12, Bruker AXS, Inc., 2002). All non-hydrogen atoms were refined anisotropically. Hydrogen atoms were placed in calculated idealized positions. The compound crystallizes with half a molecule of diethyl ether per formula unit. This solvent molecule is situated on a crystallographic 2-fold axis and disordered and SIMU and ISOR restraints were applied in its refinement. The residual peak and hole electron densities were 1.839 and −0.802 e Å^{-3}. The absorption coefficient was 2.942 mm^{-1}. The least-squares refinement converged normally with residuals of R1 = 0.0696, wR2 = 0.0645, and GOF = 1.033 (all data). Crystal data: $C_{63}H_{90}N_2O_{4.5}SiU$, monoclinic, space group $C2/c$, a = 30.215(2) Å, b = 18.212(2) Å, c = 23.904(2) Å, β = 120.735(8)°, V = 11 306(2) Å^3, Z = 8, ρ_{calcd} = 1.426 Mg/m^3, $F(000)$ = 4992, R1(F) = 0.0324, wR2(F^2) = 0.0543 ($I > 2\sigma(I)$). CCDC reference number: CCDC 862724.

Crystallographic Details for 4. Pale green prisms, grown from cooling a saturated solution of **4** at −35 °C, were coated with isobutylene oil on a microscope slide. A crystal of approximate dimensions 0.41 × 0.30 × 0.23 mm^3 was selected and mounted on a nylon loop. A total of 59 117 reflections ($-19 \le h \le 19$, $-19 \le k \le 19$, $-19 \le l \le 19$) were collected at T = 150(2) K in the θ range from 3.53 to 27.88°, 13 235 of which were unique (R_{int} = 0.0662) and 11 087 were observed ($I > 2\sigma(I)$) on a Bruker-Nonius KappaCCD diffractometer using Mo Kα radiation (λ = 0.710 73 Å, graphite monochromator). The structure was solved by direct methods and refined by full-matrix least-squares procedures on F^2 (SHELXTL NT 6.12, Bruker AXS, Inc., 2002). The compound crystallizes with one molecule of DME per formula unit. All non-hydrogen atoms were refined anisotropically. Hydrogen atoms were placed in calculated idealized positions. The residual peak and hole electron densities were 2.309 and −1.338 e Å^{-3}. The absorption coefficient was 2.968 mm^{-1}. The least-squares refinement converged normally with residuals of R1 = 0.0534, wR2 = 0.0782, and GOF = 1.106 (all data). Crystal data: $C_{62}H_{86}N_4O_7U$, triclinic, space group $P\bar{1}$, a = 14.4624(8) Å, b = 14.791(2) Å, c = 15.032(2) Å, α = 65.803(9)°, β = 83.783(7)°, γ = 71.972(5)°, V = 2788.3(5) Å^3, Z = 2, ρ_{calcd} = 1.474 Mg/m^3, $F(000)$ = 1268, R1(F) = 0.0353, wR2(F^2) = 0.0711 ($I > 2\sigma(I)$). CCDC reference number: CCDC 862725.

■ ASSOCIATED CONTENT

Ⓢ Supporting Information

Calculation details and tables. This material is available free of charge via the Internet at http://pubs.acs.org.

■ AUTHOR INFORMATION

Corresponding Author

*E-mail: wolfgang.hieringer@chemie.uni-erlangen.de (W.H.); karsten.meyer@chemie.uni-erlangen.de (K.M.).

Notes

The authors declare no competing financial interest.

■ ACKNOWLEDGMENTS

This work was supported by the Bundesministerium für Bildung und Forschung (BMBF 2020+, 02NUK012B), the Deutsche Forschungsgemeinschaft within SFB583, and by the Cluster of Excellence "Engineering of Advanced Materials" granted to the University of Erlangen. The FAU Erlangen-Nuremberg is gratefully acknowledged for financial support, as is COST Action CM1006.

■ REFERENCES

(1) (a) Cenini, S.; Gallo, E.; Caselli, A.; Ragaini, F.; Fantauzzi, S.; Piangiolino, C. *Coord. Chem. Rev.* **2006**, *250*, 1234−1253. (b) Ren, W.; Zi, G.; Walter, M. D. *Organometallics* **2012**, *31*, 672−679.

(2) (a) Dehnicke, K.; Strähle, J. *Angew. Chem., Int. Ed.* **1992**, *31*, 955−978. (b) Tornieporth-Oetting, I. C.; Klapötke, T. M. *Angew. Chem., Int. Ed.* **1995**, *34*, 511−520.

(3) (a) Korobkov, I.; Gambarotta, S.; Yap, G. P. A. *Angew. Chem., Int. Ed.* **2002**, *41*, 3433−3436. (b) Evans, W. J.; Kozimor, S. A.; Ziller, J. W. *Science* **2005**, *309*, 1835−1838. (c) Evans, W. J.; Miller, K. A.; Ziller, J. W.; Greaves, J. *Inorg. Chem.* **2007**, *46*, 8008−8018. (d) Nocton, G.; Pécaut, J.; Mazzanti, M. *Angew. Chem., Int. Ed.* **2008**, *47*, 3040−3042.

(4) Thetford, R.; Mignanelli, M. *J. Nucl. Mater.* **2003**, *320*, 44−53.

(5) Fox, A. R.; Cummins, C. C. *J. Am. Chem. Soc.* **2009**, *131*, 5716−5717.

(6) Fox, A. R.; Arnold, P. L.; Cummins, C. C. *J. Am. Chem. Soc.* **2010**, *132*, 3250−3251.

(7) Thomson, R. K.; Cantat, T.; Scott, B. L.; Morris, D. E.; Batista, E. R.; Kiplinger, J. L. *Nature Chem.* **2010**, *2*, 723−729.

(8) (a) Chermette, H.; Rachedi, K.; Volatron, F. *J. Mol. Struct. (THEOCHEM)* **2006**, *762*, 109−121. (b) Coe, B. J.; Glenwright, S. J. *Coord. Chem. Rev.* **2000**, *203*, 5−80.

(9) Denning, R. G., *Electronic Structure and Bonding in Actinyl Ions*; Springer: Berlin, 1992; Vol. 79.

(10) (a) Bendix, J.; Bøgevig, A. *Inorg. Chem.* **1998**, *37*, 5992−6001. (b) Griffith, W. P. *J. Chem. Soc. A* **1969**, 211−218.

(11) (a) de Wet, J. F.; du Preez, J. G. H. *J. Chem. Soc., Dalton Trans.* **1978**, 592−597. (b) Bartleet, J. M.; Denning, R. G.; Morrison, I. D. *Mol. Phys.* **1992**, *75*, 601−612. (c) Brown, D.; Reynolds, C. T.; Moseley, P. T. *J. Chem. Soc., Dalton Trans.* **1972**, 857−859.

(12) (a) Randaccio, L.; Geremia, S.; Nardin, G.; Wuerges, J. *Coord. Chem. Rev.* **2006**, *250*, 1332−1350. (b) Kuta, J.; Wuerges, J.; Randaccio, L.; Kozlowski, P. M. *J. Phys. Chem. A* **2009**, *113*, 11604−11612.

(13) O'Grady, E.; Kaltsoyannis, N. *Dalton Trans.* **2002**, 1233−1239.

(14) Kovács, A.; Konings, R. J. M. *Chem. Phys. Chem.* **2006**, *7*, 455−462.

(15) (a) Straka, M.; Dyall, K. M.; Pyykkö, P. *Theor. Chem. Acc.* **2001**, *106*, 393−403. (b) García-Hernández, M.; Lauterbach, C.; Krüger, S.; Matveev, A.; Rösch, N. *J. Comput. Chem.* **2002**, *23*, 834−846. (c) Vetere, V.; Maldivi, P.; Adamo, C. *J. Comput. Chem.* **2003**, *24*, 850−858. (d) Batista, E. R.; Martin, R. L.; Hay, P. J. *J. Chem. Phys.* **2004**, *121*, 11104−11111. (e) Iché-Tarrat, N.; Marsden, C. J. *J. Phys. Chem. A* **2008**, *112*, 7632−7642. (f) Schreckenbach, G.; Shamov, G. A. *Acc. Chem. Res.* **2010**, *43*, 19−29. (g) Odoh, S. O.; Schreckenbach, G. *J. Phys. Chem. A* **2010**, *114*, 1957−1963.

(16) Shamov, G. A.; Schreckenbach, G.; Vo, T. N. *Chem. Eur. J.* **2007**, *13*, 4932−4947.

(17) Denning, R. G. *J. Phys. Chem. A* **2007**, *111*, 4125−4143.

(18) (a) Castro-Rodriguez, I.; Meyer, K. *Chem. Commun.* **2006**, 1353−1368. (b) Bart, S. C.; Anthon, C.; Heinemann, F. W.; Bill, E.; Edelstein, N. M.; Meyer, K. *J. Am. Chem. Soc.* **2008**, *130*, 12536−12546.

(19) Jones, E. R.; Hendricks, M. E.; Stone, J. A.; Karraker, D. G. *J. Chem. Phys.* **1974**, *60*, 2088−2094.

(20) Castro-Rodriguez, I.; Olsen, K.; Gantzel, P.; Meyer, K. *J. Am. Chem. Soc.* **2003**, *125*, 4565−4571.

(21) Castro-Rodriguez, I.; Nakai, H.; Zakharov, L. N.; Rheingold, A. L.; Meyer, K. *Science* **2004**, *305*, 1757−1760.

(22) Boudreaux, E. A.; Mulay, L. N., *Theory and Applications of Molecular Paramagnetism*; Wiley: New York, 1976; Vol. 510.

(23) (a) Zi, G.; Jia, L.; Werkema, E. L.; Walter, M. D.; Gottfriedsen, J. P.; Andersen, R. A. *Organometallics* **2005**, *24*, 4251−4264. (b) Crawford, M.-J.; Ellern, A.; Mayer, P. *Angew. Chem., Int. Ed.* **2005**, *44*, 7874−7878.

(24) (a) Avens, L. R.; Bott, S. G.; Clark, D. L.; Sattelberger, A. P.; Watkin, J. G.; Zwick, B. D. *Inorg. Chem.* **1994**, *33*, 2248−2256. (b) Clark, D. L.; Sattelberger, A. P.; Andersen, R. A. *Inorg. Synth* **1997**, *31*, 307. (c) Clark, D.; Sattelberger, A. P.; Bott, S. G.; Vrtis, R. N. *Inorg. Chem.* **1989**, *28*, 1771−1773. (d) Lam, O. P.; Bart, S. C.; Kameo, H.; Heinemann, F. W.; Meyer, K. *Chem. Commun.* **2010**, *46*, 3137−3139.

(25) Spencer, L. P.; Altwer, R.; Wei, P.; Gelmini, L.; Gauld, J.; Stephan, D. W. *Organometallics* **2003**, *22*, 3841−3854.
(26) (a) Ahlrichs, R.; Bär, M.; Häser, M.; Horn, H.; Kölmel, C. *Chem. Phys. Lett.* **1989**, *162*, 165. (b) Ahlrichs, R.; Furche F.; Hättig C.; Klopper W. M.; Sierka, M.; Weigend, F. Turbomole version 5.10, University of Karlsruhe, since 1989; www.turbomole.com.
(27) (a) te Velde, G.; Bickelhaupt, F. M.; van Gisbergen, S. J. A.; Fonseca Guerra, C.; Baerends, E. J.; Snijders, J. G.; Ziegler, T. *J. Comput. Chem.* **2001**, *22*, 931−967. (b) Baerends, E. J., et al. Amsterdam Density Functional Program (ADF) version 2010.01, Amsterdam, since 1978; www.scm.com.
(28) (a) Becke, A. D. *Phys. Rev. A* **1988**, *38*, 3098. (b) Perdew, J. P. *Phys. Rev. B* **1986**, *33* (12), 8822.
(29) Perdew, J. P.; Burke, K.; Ernzerhoff, M. *Phys. Rev. Lett.* **1996**, *77*, 3865.
(30) Tao, J.; Perdew, J. P.; Staroverov, V. N.; Scuseria, G. E. *Phys. Rev. Lett.* **2003**, *91*, 146401.
(31) Grimme, S. *J. Comput. Chem.* **2006**, *27*, 1787−1799.
(32) Staroverov, V. N.; Scuseria, G. E.; Tao, J.; Perdew, J. P. *J. Chem. Phys.* **2003**, *119*, 12129.
(33) (a) Becke, A. D. *J. Chem. Phys.* **1993**, *98*, 5648. (b) Stephens, P. J.; Devlin, F. J.; Chabalowski, C. F.; Frisch, M. J. *J. Phys. Chem.* **1994**, *98*, 11623−11627.
(34) (a) Ernzerhof, M.; Scuseria, G. E. *J. Chem. Phys.* **1999**, *110*, 5029. (b) Adamo, C.; Barone, V. *J. Chem. Phys.* **1999**, *110*, 6158.
(35) (a) Weigend, F. *Phys. Chem. Chem. Phys.* **2006**, *8*, 1057−1065. (b) Weigend, F.; Ahlrichs, R. *Phys. Chem. Chem. Phys.* **2005**, *7*, 3297−3305.
(36) (a) Küchle, W.; Dolg, M.; Stoll, H.; Preuss, H. *J. Chem. Phys.* **1994**, *100*, 7535. (b) Cao, X.; Dolg, M. *J. Mol. Struct. (THEOCHEM)* **2004**, *673*, 203−209. (c) Andrae, D.; Häussermann, U.; Dolg, M.; Stoll, H.; Preuss, H. *Theor. Chim. Acta* **1990**, *77*, 123.
(37) (a) Eichkorn, K.; Treutler, O.; Öhm, H.; Häser, M.; Ahlrichs, R. *Chem. Phys. Lett.* **1995**, *240*, 283−290. (b) Sierka, M.; Hogekamp, A.; Ahlrichs, R. *J. Chem. Phys.* **2003**, *118*, 9136.
(38) Van Lenthe, E.; Baerends, E. J.; Snijders, J. G. *J. Chem. Phys.* **1993**, *99*, 4597−4610.